CHEMISTRY
AN ASIAN JOURNAL

DOI: 10.1002/asia.201200222

Nanowire Transistor-Based Ultrasensitive Virus Detection with Reversible Surface Functionalization

Pei-Ling Chiang,[a, b] Tzu-Chi Chou,[a] Tzu-Heng Wu,[a, b] Chang-Chi Li,[a, b] Chun-Da Liao,[a, b] Jeng-Yu Lin,[b] Ming-Hsueh Tsai,[a, b] Chia-Chang Tsai,[a, b] Chih-Jung Sun,[a, b] Ching-Ho Wang,[c] Jim-Min Fang,*[a, d] and Yit-Tsong Chen*[a, b]

Abstract: We have applied a reusable silicon nanowire field-effect transistor (SiNW-FET) as a biosensor to conduct ultrasensitive detection of H5N2 avian influenza virus (AIV) in very dilute solution. The reversible surface functionalization of SiNW-FET was made possible using a disulfide linker. In the surface functionalization, 3-mercaptopropyltrimethoxysilane (MPTMS) was first modified on the SiNW-FET (referred to as MPTMS/SiNW-FET), with subsequent dithiothreitol washing to reduce any possible disulfide bonding between the thiol groups of MPTMS. Subsequently, receptor molecules could be immobilized on the MPTMS/SiNW-FET by the formation of a disulfide bond. The success of the reversible surface functionalization was verified with fluorescence examination and electrical measurements. A surface topograph of the SiNW-FET biosensor modified with a monoclonal antibody against H5N2 virus (referred to as mAb_{H5}/SiNW-FET) after detecting approximately 10^{-17} M H5N2 AIVs was scanned by atomic force microscopy to demonstrate that the SiNW-FET is capable of detecting very few H5N2 AIV particles.

Keywords: biosensors · nanowires · reversible surface functionalization · viruses

Introduction

Influenza viruses of types A, B, and C belong to the Orthomyxoviridae family of RNA viruses and are further classified into several subtypes based on two glycoproteins, hemagglutinin (HA) and neuraminidase (NA), located on the surfaces of the viruses.[1] According to the statistical figures for the worldwide pandemic outbreak of highly pathogenic H5N1 avian influenza virus (AIV) in the past eight years, 59% of the 539 infected humans died.[2] Although the number of recent casualties bears no comparison to the outbreak at the beginning of the 20th century, the case death rate is much higher now than before.[3] To prevent a potentially hazardous AIV outbreak, a sensitive and rapid analysis platform to establish a public health alarm system is mandatory. To date, several methods have been used to confirm AIV infection, including immunofluorescence assay (IFA), hemagglutination-inhibition (HI), enzyme immunoassays (EIA), and reverse transcription polymerase chain reaction (RT-PCR).[4] Among them, the EIA-based techniques, mostly targeting the abundant nucleoprotein in influenza virus, are simple and convenient but cannot distinguish the HA subtypes. RT-PCR has the best sensitivity; however, choosing the proper primer sets becomes more challenging due to the diverse virus subtypes and the continuing evolution of AIVs.

The development of the silicon nanowire field-effect transistor (SiNW-FET) as a sensorial tool has significant impact on the fields of chemical and biological analysis,[5] biomedical diagnosis,[6] and cellular research,[7] because of its ultrasensitive, label-free, rapid screening and real-time detecting capabilities.[8] Herein, we applied a SiNW-FET to detect H5N2 AIV particles (A/duck/Yunlin/04) with an emphasis on the reversible surface functionalization of the SiNW via a disulfide linker, rendering the SiNW-FET a reusable device for fast screening of H5N2 AIV. In the previous applications of SiNW-FETs that were focused on detection of specific antigens, the corresponding antibody was generally functionalized onto the SiNW-FET through covalent bonding, where silane aldehyde was commonly adapted as

[a] P.-L. Chiang, T.-C. Chou, T.-H. Wu, C.-C. Li, Dr. C.-D. Liao, M.-H. Tsai, Dr. C.-C. Tsai, C.-J. Sun, Prof. Dr. J.-M. Fang, Prof. Dr. Y.-T. Chen
Department of Chemistry, National Taiwan University
No. 1, Sec. 4, Roosevelt Road, Taipei, 10617 Taiwan (R.O.C)
Fax: (+886) 2-2363-6359
Fax: (+886) 2-2363-7812
E-mail: jmfang@ntu.edu.tw
ytcchem@ntu.edu.tw

[b] P.-L. Chiang, T.-H. Wu, C.-C. Li, Dr. C.-D. Liao, Dr. J.-Y. Lin, M.-H. Tsai, Dr. C.-C. Tsai, C.-J. Sun, Prof. Dr. Y.-T. Chen
Institute of Atomic and Molecular Sciences, Academia Sinica
P. O. Box 23-166, Taipei 106, Taiwan (R.O.C)

[c] Prof. Dr. C.-H. Wang
Department of Veterinary Medicine
National Taiwan University
No. 1, Sec. 4, Roosevelt Road, Taipei, 10617 Taiwan (R.O.C)

[d] Prof. Dr. J.-M. Fang
The Genomics Research Center, Academia Sinica
P. O. Box 23-166, Taipei 106, Taiwan (R.O.C)

Supporting information for this article is available on the WWW under http://dx.doi.org/10.1002/asia.201200222.

a linker to anchor the antibody onto the SiNW-FET.[9] However, once silane aldehyde was linked with the antibody via reductive amination, it was difficult to reverse the amine linkage back to its original free aldehyde state after the antigen detection. As a result, it was problematic to remove the tightly bound antigen–antibody complex, yielding a device that could only be used for a single measurement. Strong oxidants might be able to cleave the amine linkage, but this is unlikely without damaging the device. By judiciously selecting a reversible functionalization method to anchor an antibody onto a SiNW-FET via a disulfide bond, we show in the present study that this sensorial device is reusable by reducing the disulfide bond with dithiothreitol (DTT), while concurrently removing the antibody–virus complex. This reversible surface functionalization by reducing disulfide bonds is comparable with our other recently developed technique of modifying the surface of a SiNW-FET with the reversible association–dissociation between glutathione (GSH) and glutathione *S*-transferase (GST)-tagged protein,[5g,6e] allowing the sensitive SiNW-FET to serve as a reusable and high-throughput biosensor for the fast screening of protein–protein interactions under physiological conditions. However, from the use of the GSH–GST reversible system, the GST (a protein of ca. 2.5 nm in size)[10] located between the target–receptor complex and SiNW might partly screen the interaction field exerted from the target–receptor complex to the SiNW-FET, thus reducing the acquired signal. In contrast to the sizable GST, the advantage of applying the simple disulfide bond as a chemical linker for the immobilization of a receptor protein onto the SiNW-FET surface could minimize this detrimental field-shielding effect.

Herein, we first demonstrated a reusable SiNW-FET device through the reversible functionalization of biotin on the SiNW-FET surface via a disulfide linker. This reusable SiNW-FET was then modified with a monoclonal antibody against H5N2 virus (mAbH5) to detect H5N2 AIV at very dilute concentrations. Meanwhile, we also showed the binding specificity of the mAbH5-modified SiNW-FET (referred to as mAb_{H5}/SiNW-FET). From the surface topograph of the SiNW-FET after detecting approximately 10^{-17} M H5N2 AIVs, we verified that the sensitive SiNW-FET is capable of detecting very few H5N2 AIV particles. This reversible surface-modification technique via a disulfide linker can also be applied to other field-effect transistors, such as organic thin-film transistors[11] and graphene-FETs.[12] By properly selecting a thiol-containing chemical linker to be modified on organic thin film transistors, or graphene-FETs, the transistor-based biosensors can function as reusable sensing devices as well.

Results and Discussion

Figure 1 shows the schematic illustration and experimental demonstration for the reversible surface functionalization of a SiNW-FET via a disulfide linker. First, 1% MPTMS in ethanol was pumped into a polydimethylsiloxane (PDMS) microfluidic channel, which was designed to couple with the SiNW-FET device arrays (Figure 1a). After the SiNW-FET was modified with 3-mercaptopropyltrimethoxysilane (MPTMS) to form a MPTMS/SiNW-FET (Figure 1b), ethanol was introduced into the PDMS microfluidic channel to wash the FET devices, followed by DTT in phosphate buffered saline (1×PBS) to reduce any possible disulfide bonding between the thiol groups of MPTMS. The MPTMS/SiNW-FET was then flushed with 1×PBS. Next, the receptor molecules could be immobilized on the SiNW-FET via the formation of a disulfide bond with the MPTMS/SiNW-FET.

To demonstrate the reversible functionalization on the MPTMS/SiNW-FET surface through a disulfide linker, *N*-(6-(biotinamido)hexyl)-3′-(2′-pyridyldithio)-propionamide (biotin-HPDP) was immobilized on the MPTMS/SiNW-FET to make a biotin/SiNW-FET (Figure 1b); subsequently, the biotin moiety was removed with DTT to return the device surface to MPTMS/SiNW-FET. Figure 1c shows an electrical measurement to verify the reversibility between MPTMS/SiNW-FET and biotin/SiNW-FET, involving the processes of 1) the formation of MPTMS/SiNW-FET, 2) the immersion of MPTMS/SiNW-FET in 1×PBS, 3) the reaction of biotin-HPDP with MPTMS/SiNW-FET to form a biotin/SiNW-FET, and 4) the removal of biotin with DTT to return the device to MPTMS/SiNW-FET. In the course of the electrical measurement, three reproducible cycles were observed to demonstrate the reusability of the SiNW-FET device via a disulfide linker. Typically, a MPTMS/SiNW-FET can be used repetitively for more than 20 cycles.

Using this reversible surface functionalization method, we further made a reusable SiNW-FET for the H5N2 AIV detection, as represented schematically in Figure 2a. One advantage of choosing a disulfide linker for the reversible surface functionalization on a SiNW-FET is that the immobilization reaction of receptor proteins (such as AIV–mAb_{H5} in this study) through the disulfide bond can be carried out conveniently at room temperature to avoid spoiling the normal functions of proteins or damaging the SiNW-FET device, which could occur if the reaction would otherwise be conducted at escalated temperature. Shown in Figure 2b are the electrical responses of a SiNW-FET in the processes of preparing the MPTMS/SiNW-FET with 500 mM DTT washing, 1× PBS flushing, mAb_{H5} immobilization, and another cycle of renewing the surface functionalization initiated with DTT washing. It is noted that the conductance of the SiNW-FET remained at the original level (the horizontal dashed line) after the cleavage of disulfide bonds followed by 1× PBS flushing, again indicating that the device surface was returned to the MPTMS/SiNW-FET state without analyte contamination and was ready for the next round of measurement.

The successful immobilization of mAb_{H5} on a Si substrate was also corroborated with a microfluorescence technique. As shown in Figure 2c, the fluorescent pattern was obtained by attaching an anti-chicken IgG fluorescein isothiocyanate conjugate (FITC-Ab) to a MPTMS-modified micropattern with the same modification procedures as described in Fig-

CHEMISTRY
AN ASIAN JOURNAL

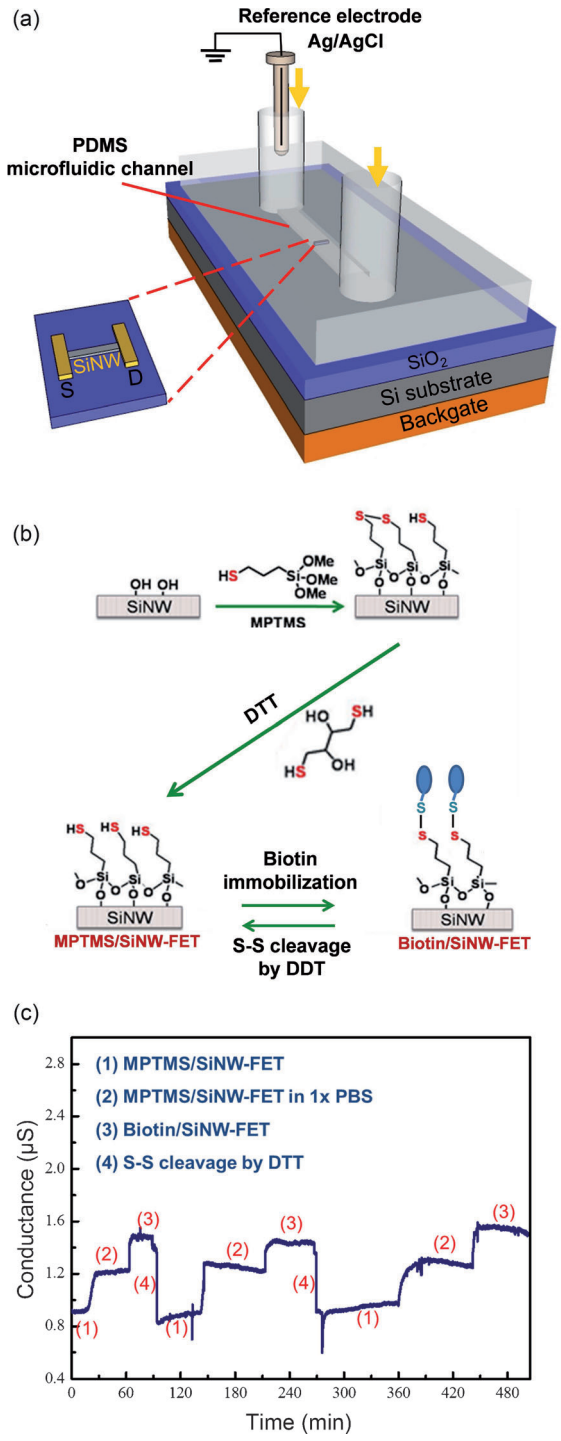

Figure 1. Reversible surface functionalization on a SiNW-FET via a disulfide linker. a) An illustration shows the experimental setup of a SiNW-FET system. A PDMS microfluidic channel was designed to couple the SiNW-FET arrays to guide the flow of sample solution. An Ag/AgCl electrode was used as a solution gate. b) A schematic diagram illustrates that the surface of a SiNW-FET was first modified with MPTMS and then washed with DTT to form a MPTMS/SiNW-FET. To demonstrate the reversible surface functionalization, biotin-HPDP was immobilized on the MPTMS/SiNW-FET (referred to as biotin/SiNW-FET) through a disulfide linker; the disulfide bond was subsequently cleaved with DTT to return the device surface to MPTMS/SiNW-FET. c) An electrical measurement verified the reversible surface functionalization between MPTMS/SiNW-FET and biotin/SiNW-FET, including the steps of 1) a MPTMS/SiNW-FET after DTT washing, 2) the MPTMS/SiNW-FET immersed in 1× PBS and then in reaction with biotin-HPDP to form 3) biotin/SiNW-FET via a disulfide bond, and 4) the removal of biotin by DTT washing to return the device to MPTMS/SiNW-FET. Three reproducible cycles in the electrical measurement demonstrate the reusablility of a SiNW-FET device.

ure 2a. The illuminating pattern is in sharp contrast with the dark unmodified surroundings, which also indicates that there is no significant nonspecific adhesion on the Si surface without modification. After the removal of FITC-Ab by DTT washing, the blank image in Figure 2d was obtained, thus demonstrating the complete cleavage of the disulfide bonds on the Si substrate.

The ζ potential of H5N2 AIV, displayed in Figure 3, was characterized at $2.4 \leq pH \leq 8.4$. From the ζ potential measurements, the pI of H5N2 AIV was determined to be approximately 3.2. In addition, the transmission electron microscopy (TEM) images of H5N2 AIV particles (ca. 120 nm in size) and polystyrene latex beads (137 nm in diameter) were taken for comparison (Figure 4).

In the upper trace of Figure 5a, the applicability of the mAb_{H5}/SiNW-FET to detect H5N2 AIV was tested with a sample solution of 10^7 AIV mL^{-1} (ca. 1.6×10^{-14} M) in 1× PBS, where the conductance of mAb_{H5}/SiNW-FET was stabilized in 1× PBS in the beginning and increased dramatically upon the addition of H5N2 AIV, indicating the strong binding affinity between mAb_{H5} and H5N2 AIV. The electrical enhancement in the p-type mAb_{H5}/SiNW-FET is due to a gating effect generated by the binding of the negatively charged H5N2 AIV ($pI \approx 3.2$, Figure 3) at pH 7.4. However, this device responded only slightly to the subsequent addition of 10^8 AIV mL^{-1}, suggesting that the binding sites on the mAb_{H5}/SiNW-FET could have been saturated. As a rough estimation, less than 20 AIVs could bind onto the surface of mAb_{H5}/SiNW-FET, if the sensorial device is assumed to have a SiNW (ca. 30 nm in diameter) located between the source and drain electrodes (ca. 2 μm apart). The molecular sizes for H5N2 AIV and mAb_{H5} are approximately 120 nm (Figure 4) and 8 nm,[13] respectively.

To confirm that the signals are genuinely caused by binding H5N2 AIV onto the mAb_{H5}/SiNW-FET, we conducted two negative control experiments. The lower trace of Figure 5a shows the results of a test of whether H5N2 AIV could be detected by a bare SiNW-FET without any surface modification. Before H5N2 AIV was introduced, the conductance of the SiNW-FET was balanced by immersing the SiNW-FET in 1× PBS. No significant conductance change was observed after the arrival of H5N2 AIV (10^7 AIV mL^{-1}). For comparison, we then modified mAb_{H5} on the same SiNW-FET device (i.e., to form a mAb_{H5}/SiNW-FET) to detect H5N2 AIV (10^7 AIV mL^{-1}). As shown in the inset of Figure 5a, the obvious electrical response verifies that the conductance change in the mAb_{H5}/SiNW-FET originates from the specific binding between mAb_{H5}

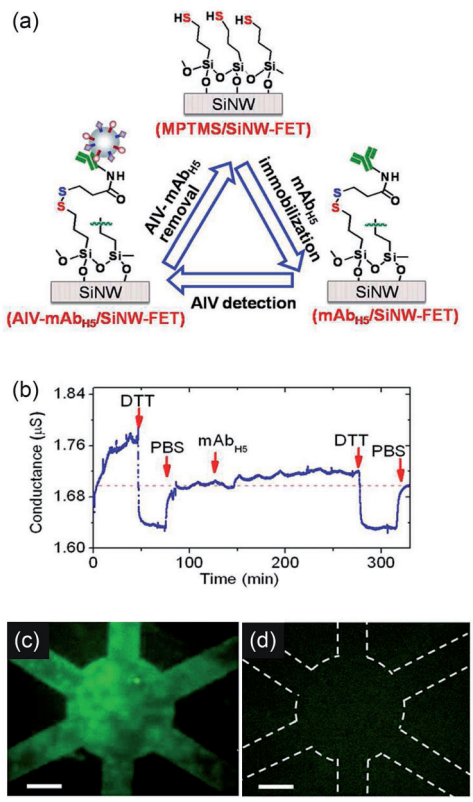

Figure 2. Corroboration of the reversible surface functionalization on a SiO_2/Si surface with electrical measurement and fluorescence examination. a) An illustration represents a reusable MPTMS/SiNW-FET for the detection of AIV by modification of mAb_{H5}. The surface of a MPTMS/SiNW-FET was modified with mAb_{H5} through a disulfide linker to give mAb_{H5}/SiNW-FET. After AIV detection, the AIV–mAb_{H5} complex on the SiNW-FET (referred to as AIV–mAb_{H5}/SiNW-FET) was removed by DTT washing to return the device to the MPTMS/SiNW-FET state. b) The reversible surface functionalization on a SiNW-FET was tested by electrical measurement. The electrical responses of a SiNW-FET include preparing the MPTMS/SiNW-FET with 500 mM DTT washing, 1×PBS flushing, mAb_{H5} immobilization, and another cycle of renewing the surface functionalization initiated by DTT washing. The horizontal dashed line marks the return of the conductance level when the SiNW-FET surface was regenerated to MPTMS/SiNW-FET. c) Fluorescence from FITC-Ab anchored on a MPTMS-modified SiO_2/Si micropattern through a disulfide linker is in sharp contrast to the dark surroundings without the modification with FITC-Ab. d) The fluorescent pattern in (c) was removed with DTT washing, demonstrating the effective breaking of disulfide bonds by DTT. The demarcation (dashed lines) highlights the pattern in (c). The scale bars in (c) and (d) are 1 μm.

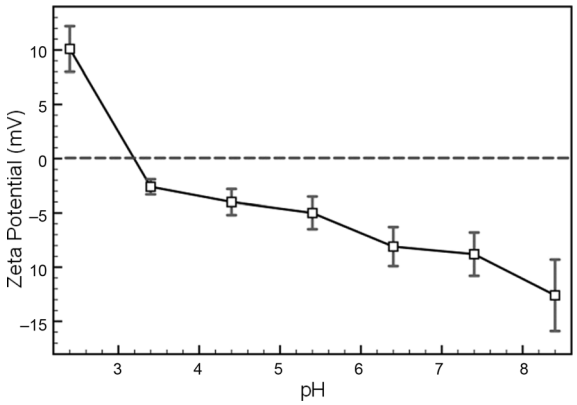

Figure 3. ζ potential of H5N2 AIV. The ζ-potentials of H5N2 AIV were measured in 1×PBS at different pH values. The allantoic samples containing H5N2 AIVs were taken directly from egg embryos and diluted 10^3-fold. Each data point was measured five times with a single standard deviation. The plot shows that the H5N2 AIV is negatively charged at pH ≥ 4.

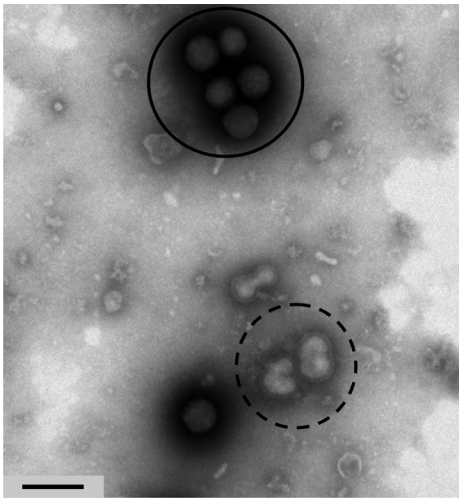

Figure 4. Molecular size of H5N2 AIV particles. A TEM image shows the distinctive shapes and morphologies of polystyrene latex particles (137 nm in diameter, solid circle) and H5N2 AIVs (dashed circle). The membrane proteins on the surface of the H5N2 AIV provide a clear contrast for distinguishing viruses from polystyrene latex particles. The size of an H5N2 AIV particle is approximately 120 nm. The scale bar represents 200 nm.

and H5N2 AIV. For another control test of the selectivity of this sensorial device, we applied mAb_{H5}/SiNW-FETs to the detection of H6N1 AIV. As displayed in Figure 5b, while there is no apparent electrical response of the mAb_{H5}/SiNW-FET to H6N1 AIV (10^8 AIV mL^{-1}), a conductance increase was observed after introducing H5N2 AIV (10^7 AIV mL^{-1}), manifesting once more the binding specificity of the mAb_{H5}/SiNW-FET. The sudden decrease of electrical conductance after introducing H5N2 AIV was caused by manually changing H6N1 AIV-containing solution to H5N2 AIV-containing solution during the electrical measurement. In Figure 5, the considerable signal collection time (minutes) for the mAb_{H5}/SiNW-FET to reach an equilibrium in binding with H5N2 AIVs stemmed from detection of very dilute sample solution (<1 fM) in the electrical measurement; accordingly, the limited number of H5N2 AIV particles needed to flow across the laminar fluid by diffusion and convection inside the PDMS microfluidic channel to reach the mAb_{H5}/SiNW-FET device surface. It is noted that without the delicately site-directed immobilization of mAb_{H5}, the attachment of mAb_{H5} via its amino groups to the SiNW-FET surface could cause a random orientation of the immobilized mAb_{H5}.[14] As a result, some of the binding sites on the immobilized mAb_{H5} could be very close to the SINW-FET surface, com-

CHEMISTRY
AN ASIAN JOURNAL

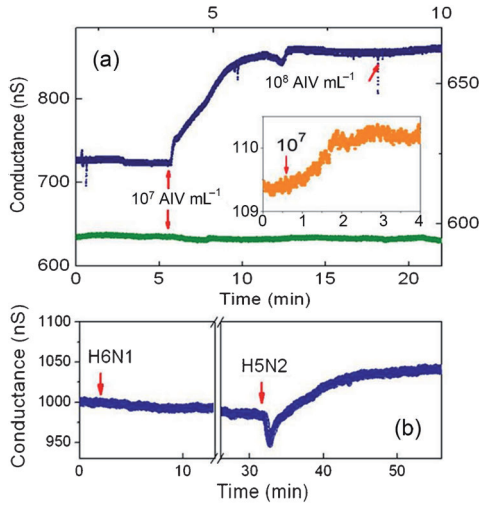

Figure 5. Real-time detection of H5N2 AIV by mAbH5/SiNW-FET. a) Upper trace: The mAbH5/SiNW-FET biosensor has a prominent electrical response to H5N2 AIV (10^7 AIV mL^{-1}), but it exhibits only a slight variation in response to the subsequent addition of 10^8 AIV mL^{-1}, probably due to a saturation on the binding sites. Arrows indicate the addition of H5N2 AIV. Lower trace: A negative control was developed by applying a bare SiNW-FET without any surface modification for detection of H5N2 AIV. No significant conductance change was monitored after the addition of H5N2 AIV (10^7 AIV mL^{-1}). Inset: In contrast, after the bare SiNW-FET was modified with mAbH5 for detection of H5N2 AIV (10^7 AIV mL^{-1}), an apparent conductance change was observed. b) Another control test was carried out using a mAbH5/SiNW-FET to probe H6N1 AIV (10^8 AIV mL^{-1}). While there is no apparent electrical response to H6N1 AIV, a conductance increase was observed after introducing H5N2 AIV (10^7 AIV mL^{-1}), illustrating the binding specificity of mAbH5/SiNW-FET.

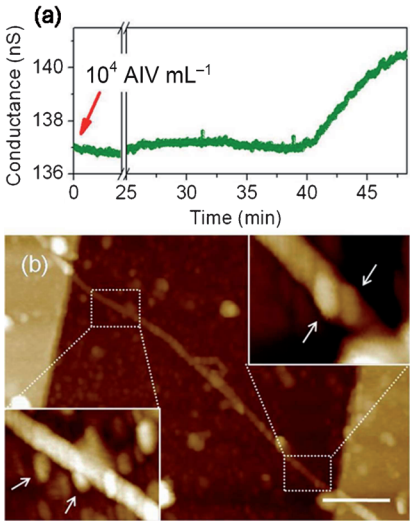

Figure 6. H5N2 AIVs bound on a mAbH5/SiNW-FET examined with electrical measurements and by AFM topography. a) A prominent conductance change in the mAbH5/SiNW-FET was observed after more than 40 min of collecting H5N2 AIVs (10^4 AIV mL^{-1}) with a flow rate of 500 μL h^{-1}. b) An AFM topograph of H5N2 AIVs bound on the mAbH5/SiNW-FET was taken soon after the electrical measurement of (a) was finished. The expanded scales for the bound H5N2 AIVs are displayed in the insets, where H5N2 AIV particles are marked with white arrows. The size of an H5N2 AIV (ca. 120 nm) is comparable to that observed by TEM imaging in Figure 4. The scale bar represents 1 μm.

parable to the Debye–Hückel screening length of the buffer solution used.

As for the speculation that binding only a limited number of H5N2 AIVs on the mAb_{H5}/SiNW-FET could have caused an electrical response in this biosensor, we attempted to observe the AIV–mAb_{H5} complex on the SiNW-FET surface by atomic force microscopy (AFM) after a biosensing measurement. Figure 6a shows a typical electrical measurement for detecting very dilute H5N2 AIVs (10^4 AIV mL^{-1}, ca. 1.6×10^{-17} M) with a flow rate of 500 μL h^{-1}. Because of this extremely small number density (10^4 AIV mL^{-1}) of H5N2 AIVs, a long response time of over 40 min was needed for the signal detection in the electrical measurement. Figure 6b displays the AFM surface topograph of the AIV–mAb_{H5}/SiNW-FET, scanned right after the electrical measurement shown in Figure 6a. The image confirms that only a very small number of H5N2 AIVs bound to the mAb_{H5}/SiNW-FET, and the virus size of approximately 120 nm is consistent with that obtained from TEM imaging (Figure 4). In this AFM topographic investigation, the surface images before and after the electrical measurements were taken (i.e. mAb_{H5}/SiNW-FET and AIV–mAb_{H5}/SiNW-FET, respectively) to distinguish H5N2 AIV from any possible aggregated mAb_{H5} (picture not shown). The prominent signal-to-noise ratio (S/N ≈ 18) in Figure 6a caused by very few H5N2 AIV particles bound to the mAb_{H5}/SiNW-FET (Figure 6b) indicates that this SiNW-FET biosensor can serve as a powerful molecular recognition and sensing platform for ultrasensitive biomolecular detection.

Conclusions

We have demonstrated the ultrasensitive detection of H5N2 AIV using a reusable SiNW-FET, which was made possible by the reversible surface functionalization on the SiNW via a disulfide linker. The success of the reversible surface functionalization was verified by electrical and microfluorescence examinations. Detections of very dilute H5N2 AIV at 10^{-12}–10^{-17} M were achieved. After the biosensing experiments, the very few bound H5N2 AIVs on the surface of the mAb_{H5}/SiNW-FET were investigated by AFM topography, demonstrating the ultrasensitivity of SiNW-FETs in biosensing measurements. The demonstrative performance of this reusable biosensor makes SiNW-FET a good candidate for fast high-throughput screening of proteins, DNA sequences, small molecules, cancer biomarkers, and viruses.[8d] In particular, the SiNW-FET biosensors can be advanced as a powerful tool for future biomedical applications, such as virus infection diagnosis and early cancer detection.

Experimental Section

The chemical and biological materials used in the experiments are listed in Supporting Information S1. SiNWs were synthesized from a chemical-vapor-deposition reaction assisted with catalytic Au nanoparticles (Sup-

porting Information S2) and the SiNW-FET devices were fabricated following a standard photolithographic procedure (Supporting Information S3). The experimental details for the SiNWs synthesis and SiNW-FET fabrication can be found in our previous publications.[6e,15]

Surface Functionalization

Figure 1 shows the schematic illustration and experimental demonstration for the reversible surface functionalization via a disulfide linker. In the beginning, 1% MPTMS in ethanol was pumped into a PDMS microfluidic channel ($6.25\times0.5\times0.05$ mm^3), which was designed to couple with the SiNW-FET device arrays, at a flow rate of 300 μL h^{-1} for 30 min by a syringe pump (KD Scientific, KD-101). After MPTMS was modified on the SiNW-FET to form the MPTMS/SiNW-FET, ethanol was guided into the PDMS microfluidic channel to wash the FET devices for 10 min, followed by 500 mM DTT in 1×PBS (containing 138 mM NaCl, 2.7 mM KCl, 8 mM Na_2HPO_4, 1.5 mM KH_2PO_4, pH 7.4 with NaOH) for 30 min to reduce any possible disulfide bonding between the thiol groups of MPTMS. The MPTMS/SiNW-FET was then flushed with 1×PBS for 20 min.

Next, the receptor molecules could be immobilized on the SiNW-FET via the formation of a disulfide bond with the MPTMS/SiNW-FET. In a test of the reversible surface functionalization of a SiNW-FET (as represented in Figure 1b), 0.4 mM biotin–HPDP was pumped into the PDMS microfluidic channel at 0.4 mL h^{-1} for 30 min to react with the MPTMS/SiNW-FET to form a biotin/SiNW-FET. For the H5N2 AIV detection, we first mixed mAb_{H5} (3 μL) with *N*-succinimidyl-3-(2-pyridyldithio)propionate (SPDP, 2 μL) in a vial at room temperature for 30 min, in which mAb_{H5} was linked to SPDP through the formation of an amide bond by substituting the *N*-hydroxysuccinimide of SPDP with an amine group of mAb_{H5}. Subsequently (as illustrated in Figure 2a), this mAb_{H5}-containing solution was added to 1×PBS (45 μL) to form a mixture, which was then pumped into the PDMS microfluidic channel at 25 μL h^{-1} for two hours to immobilize the mAb_{H5} on the MPTMS/SiNW-FET by the formation of a disulfide bond. After the modification of mAb_{H5} on the SiNW-FET surface to form the mAb_{H5}/SiNW-FET, the device was washed with 1×PBS for 30 min and was then ready for AIV detection. To make the device reusable (Figure 2a), the AIV–mAb_{H5} complex was removed after each biosensing experiment by cleaving the disulfide bond with DTT (500 mM in 1×PBS) for 2 h to restore the clean surface of the MPTMS/SiNW-FET. This regenerated MPTMS/SiNW-FET was further rinsed with deionized water before the next round of measurements. Typically, a mAb_{H5}/SiNW-FET device can be repeatedly used in electrical measurements with more than five cycles.

Fluorescence Imaging

A microscopic fluorescence imaging technique was employed to corroborate the successful modifications of MPTMS and mAb_{H5} on a Si substrate. A micropattern was designed on a Si wafer (Figure 2c) and fabricated with a standard photolithographic procedure using LOR5B/S1813 photoresists.[5g,6e] After the modification of MPTMS on the patterned Si substrate, the surrounding photoresists were washed off with a PG remover at 60 °C for two hours. The procedures to anchor an anti-chicken IgG fluorescein isothiocyanate conjugate (FITC-Ab) onto the MPTMS-modified Si surface via the SPDP linker are the same as those described above for the immobilization of mAb_{H5}. Finally, a fluorescence image of the FITC-Ab anchored micropattern (Figure 2(c)) was taken with a reverse fluorescence microscope (Nikon, Eclipse TE2000-U).

Electrical Measurement

The electrical characteristics (including the plots of source–drain current vs. gate voltage (I_{sd}–V_g) and I_{sd} vs. source–drain voltage (I_{sd}-V_{sd})) of the as-fabricated SiNW-FETs are presented in Supporting Information S4. The electrical conductance of a SiNW-FET was measured at $V_{sd}=30$ mV by a detection system that combined a current preamplifier (DL Instrument, 1211) with a lock-in amplifier (Stanford Research System, SR830 DSP) operated at a modulation frequency of 79 Hz and a time constant of 100 ms.[5g,6e,7d,16] In the electrical measurements, an Ag/AgCl electrode (BAS, MF2052) coupled to the PDMS microfluidic channel was used as a solution gate (Figure 1a) and kept at ground potential throughout the real-time electrical measurements to minimize noise in the system.

Zeta (ζ) Potential

The ζ-potential of H5N2 AIV was characterized at $2.4\le pH\le8.4$ by a Zetasizer (Malvern Instruments, 3000MS), as shown in Figure 3.

H5N2 AIV Concentration

The method to determine the number density of H5N2 AIV particles was adapted following the procedures used by Zheng et al.[17] with the details described in Supporting Information S5. By counting the number ratio between H5N2 AIVs and polystyrene latex beads from 50 TEM (JEOL JEM 2010 Analytical TEM at 200 kV) images (a representative one is shown in Figure 4), the concentration of an original sample of H5N2 AIVs was estimated statistically to be approximately 10^{11} AIV mL^{-1}.

Surface Topography

The microscopic topographs on the surface of SiNW-FETs before (i.e. mAb_{H5}/SiNW-FET as shown in Figure 2a) and after (i.e. AIV–mAb_{H5}/SiNW-FET in Figure 2a) sensing H5N2 AIV (10^4 AIV mL^{-1}) were taken by AFM (Veeco, Bioscope SZ, NSIV) in tapping mode at a scan rate of 0.5 Hz.[15a]

Acknowledgements

We thank Mr. Shu-Han Yu for his help in the synthesis of SiNWs. This work was supported by the National Science Council of Taiwan under contract numbers NSC97-2627M-002-019 and NSC97-2628M-002-013-MY3. Technical support from NanoCore, the Core Facilities for Nanoscience and Nanotechnology at Academia Sinica, is acknowledged.

[1] B. Olsen, V. J. Munster, A. Wallensten, J. Waldenstrom, A. D. M. E. Osterhaus, R. A. M. Fouchier, *Science* **2006**, *312*, 384–388.
[2] In"WHO: Affected areas with confirmed cases of H5N1 avian influenza since 2003", http://gamapserver.who.int/mapLibrary/Files/Maps/Global_H5N1inHumanCUMULATIVE_FIMS_20110316.png.
[3] Y. Suzuki, *Biol. Pharm. Bull.* **2005**, *28*, 399–408.
[4] In "WHO guidelines for investigation of human cases of avian influenza A(H5N1)", **2007**, http://www.who.int/csr/resources/publications/influenza/WHO_CDS_EPR_GIP_2006_4.pdf.
[5] a) Z. Li, Y. Chen, X. Li, T. I. Kamins, K. Nauka, R. S. Williams, *Nano Lett.* **2004**, *4*, 245–247; b) W. U. Wang, C. Chen, K. H. Lin, Y. Fang, C. M. Lieber, *Proc. Natl. Acad. Sci. USA* **2005**, *102*, 3208–3212; c) Y. L. Bunimovich, Y. S. Shin, W.-S. Yeo, M. Amori, G. Kwong, J. R. Heath, *J. Am. Chem. Soc.* **2006**, *128*, 16323–16331; d) Y. Chen, X. H. Wang, M. Hong, S. Erramilli, P. Mohanty, *Sens. Actuators B* **2008**, *133*, 593–598; e) X. Wang, Y. Chen, K. A. Gibney, S. Erramilli, P. Mohanty, *Appl. Phys. Lett.* **2008**, *92*, 013903; f) N. Misra, J. A. Martinez, S. C. J. Huang, Y. M. Wang, P. Stroeve, C. P. Grigoropoulos, A. Noy, *Proc. Natl. Acad. Sci. USA* **2009**, *106*, 13780–13784; g) S. P. Lin, C. Y. Pan, K. C. Tseng, M. C. Lin, C. D. Chen, C. C. Tsai, S. H. Yu, Y. C. Sun, T. W. Lin, Y. T. Chen, *Nano Today* **2009**, *4*, 235–243; h) C. C. Wu, F. H. Ko, Y. S. Yang, D. L. Hsia, B. S. Lee, T. S. Su, *Biosens. Bioelectron.* **2009**, *25*, 820–825; i) F. Shen, M. Tan, Z. Wang, M. Yao, Z. Xu, Y. Wu, J. Wang, X. Guo, T. Zhu, *Environ. Sci. Technol.* **2011**, *45*, 7473–7480.
[6] a) F. Patolsky, G. F. Zheng, O. Hayden, M. Lakadamyali, X. W. Zhuang, C. M. Lieber, *Proc. Natl. Acad. Sci. USA* **2004**, *101*, 14017–14022; b) G. F. Zheng, F. Patolsky, Y. Cui, W. U. Wang, C. M. Lieber, *Nat. Biotechnol.* **2005**, *23*, 1294–1301; c) E. Stern, A. Vacic, N. K. Rajan, J. M. Criscione, J. Park, B. R. Ilic, D. J. Mooney, M. A. Reed, T. M. Fahmy, *Nat. Nanotechnol.* **2010**, *5*, 138–142; d) G. J. Zhang, L. Zhang, M. J. Huang, Z. H. H. Luo, G. K. I. Tay, E. J. A. Lim, T. G. Kang, Y. Chen, *Sens. Actuators B* **2010**, *146*, 138–144;

e) T. W. Lin, P. J. Hsieh, C. L. Lin, Y. Y. Fang, J. X. Yang, C. C. Tsai, P. L. Chiang, C. Y. Pan, Y. T. Chen, *Proc. Natl. Acad. Sci. USA* **2010**, *107*, 1047–1052.

[7] a) F. Patolsky, B. P. Timko, G. H. Yu, Y. Fang, A. B. Greytak, G. F. Zheng, C. M. Lieber, *Science* **2006**, *313*, 1100–1104; b) E. Stern, E. R. Steenblock, M. A. Reed, T. M. Fahmy, *Nano Lett.* **2008**, *8*, 3310–3314; c) B. Tian, T. Cohen-Karni, Q. Qing, X. Duan, P. Xie, C. M. Lieber, *Science* **2010**, *329*, 830–834; d) K.-S. Chang, C.-J. Sun, P.-L. Chiang, A.-C. Chou, M.-C. Lin, C. Liang, H.-H. Hung, Y.-H. Yeh, C.-D. Chen, C.-Y. Pan, Y.-T. Chen, *Biosens. Bioelectron.* **2012**, *31*, 137–143.

[8] a) E. Stern, J. F. Klemic, D. A. Routenberg, P. N. Wyrembak, D. B. Turner-Evans, A. D. Hamilton, D. A. LaVan, T. M. Fahmy, M. A. Reed, *Nature* **2007**, *445*, 519–522; b) W. Lu, P. Xie, C. M. Lieber, *IEEE Trans. Electron. Devices* **2008**, *55*, 2859–2876; c) B. P. Timko, T. Cohen-Karni, Q. Qing, B. Tian, C. M. Lieber, *IEEE Trans. Nanotechnol.* **2010**, *9*, 269–280; d) Y. Huang, D. Cai, P. Chen, *Anal. Chem.* **2011**, *83*, 4393–4406.

[9] F. Patolsky, G. Zheng, C. M. Lieber, *Nat. Protoc.* **2006**, *1*, 1711–1724.

[10] M. Nishida, S. Harada, S. Noguchi, Y. Satow, H. Inoue, K. Takahashi, *J. Mol. Biol.* **1998**, *281*, 135–147.

[11] a) P. Lin, F. Yan, *Adv. Mater.* **2012**, *24*, 34–51; b) P. Lin, X. T. Luo, I. M. Hsing, F. Yan, *Adv. Mater.* **2011**, *23*, 4035–4040.

[12] R. X. He, P. Lin, Z. K. Liu, H. W. Zhu, X. Z. Zhao, H. L. W. Chan, F. Yan, *Nano Lett.* **2012**, *12*, 1404–1409.

[13] L. J. Harris, S. B. Larson, K. W. Hasel, A. McPherson, *Biochemistry* **1997**, *36*, 1581–1597.

[14] W. Qian, B. Xu, L. Wu, C. Wang, Z. Song, D. Yao, Z. Lu, Y. Wei, *J. Inclusion Phenom. Macrocyclic Chem.* **1999**, *35*, 419–429.

[15] a) C. C. Tsai, P. L. Chiang, C. J. Sun, T. W. Lin, M. H. Tsai, Y. C. Chang, Y. T. Chen, *Nanotechnology* **2011**, *22*, 135503; b) Y. H. Yang, S. J. Wu, H. S. Chiu, P. I. Lin, Y. T. Chen, *J. Phys. Chem. B* **2004**, *108*, 846–852.

[16] a) C. W. Wang, C. Y. Pan, H. C. Wu, P. Y. Shih, C. C. Tsai, K. T. Liao, L. L. Lu, W. H. Hsieh, C. D. Chen, Y. T. Chen, *Small* **2007**, *3*, 1350–1355; b) C. C. Tsai, C. C. Yang, P. Y. Shih, C. S. Wu, C. D. Chen, C. Y. Pan, Y. T. Chen, *J. Phys. Chem. B* **2008**, *112*, 9165–9173.

[17] Y. Z. Zheng, R. Webb, P. F. Greenfield, S. Reid, *J. Virol. Methods* **1996**, *62*, 153–159.

Received: March 9, 2012
Revised: April 16, 2012
Published online: ■■ ▮▮, 0000

Biosensors

Pei-Ling Chiang, Tzu-Chi Chou, Tzu-Heng Wu, Chang-Chi Li, Chun-Da Liao, Jeng-Yu Lin, Ming-Hsueh Tsai, Chia-Chang Tsai, Chih-Jung Sun, Ching-Ho Wang, Jim-Min Fang, Yit-Tsong Chen** ____ ▮▮▮▮–▮▮▮▮

Nanowire Transistor-Based Ultrasensitive Virus Detection with Reversible Surface Functionalization

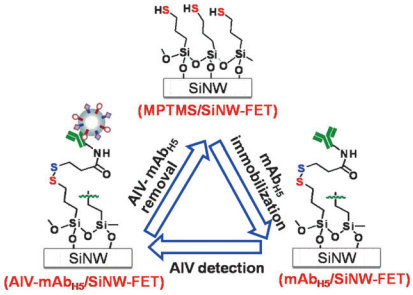

Catching the flu: The surface of a silicon nanowire field-effect transistor (SiNW-FET) is functionalized with a mercaptosilane, which forms a disulfide bond to a monoclonal antibody against avian influenza virus (AIV). This mAb$_{H5}$/SiNW-FET device shows an electrical response when the virus is bound. The sensor can be regenerated by cleaving the disulfide bond to release the antibody–virus complex and adding another portion of antibody.

